

# Arbitrary High Order WENO Finite Volume Scheme with Flux Globalization for Moving Equilibria Preservation

Mirco Ciallella<sup>(1)</sup>, Davide Torlo<sup>(2)</sup> and Mario Ricchiuto<sup>(1)</sup>

(1): Team CARDAMOM, INRIA, Univ. Bordeaux, CNRS, Bordeaux INP, IMB, UMR 5251, France

(2): SISSA mathLab, Mathematics Area, SISSA, via Bonomea 265, Trieste 34136, Italy

May 27, 2022

## Abstract

In the context of preserving stationary states, e.g. lake at rest and moving equilibria, a new formulation of the shallow water system, called Flux Globalization has been introduced by Cheng *et al.* (2019). This approach consists in including the integral of the source term in the *global flux* and reconstructing the new *global flux* rather than the conservative variables. The resulting scheme is able to preserve a large family of smooth and discontinuous steady state moving equilibria. In this work, we focus on an arbitrary high order WENO Finite Volume (FV) generalization of the global flux approach. The most delicate aspect of the algorithm is the appropriate definition of the *source flux* (integral of the source term) and the quadrature strategy used to match it with the WENO reconstruction of the hyperbolic flux. When this construction is correctly done, one can show that the resulting WENO FV scheme admits exact discrete steady states characterized by constant global fluxes. We also show that, by an appropriate quadrature strategy for the source, we can embed exactly some particular steady states, e.g. the lake at rest for the shallow water equations. It can be shown that an exact approximation of global fluxes leads to a scheme with better convergence properties and improved solutions. The novel method has been tested and validated on classical cases: subcritical, supercritical and transcritical flows.

*Keywords:* Flux Globalization, WENO, well-balanced, moving equilibria, shallow water.

## 1 Introduction

Water waves can be modeled with various systems of equations. The Saint-Venant system [16] of shallow water equations is widely used to simulate water waves in regimes where the wave lengths are larger than the water height. These equations are a system of balance laws that models the conservation of mass and momentum under the force of gravity, taking also care of the bottom topography effects through a source term. Their applications range between coastal waves, rivers, seas, lakes, tsunamis, and so on. In this work we will consider the Saint-Venant equations with a friction term.

Analytical solutions of these equations are not always available and it is necessary to recur to numerical simulations in order to approximate the exact solutions. In the past, many techniques have been used to discretize these equations: finite volume methods [6, 35, 25, 33, 14], finite element methods [39, 38, 37, 36, 4], discontinuous Galerkin [29, 5, 30] and so on. The goal of such methods is to accurately approximate the solutions with as little as possible computational costs. To achieve this, many strategies have been adopted. High order methods are a clear example of a technique to obtain more accurate results within the same dimension of the semidiscretized system. In particular, in this work we will consider the WENO high order reconstruction finite volume method to obtain (arbitrarily) high order spatial discretizations [40, 41], while for the temporal discretization we will use the Deferred Correction [15, 19, 34, 1, 23], an (arbitrarily) high order time integration method.

Another way to obtain accurate results with low computational costs is to design methods which are capable of preserving some physical properties. The shallow water equations, for example, are verified by some steady state solutions that are very easily described. The simplest equilibrium is the lake at rest steady state where the water level is constant and velocity is zero. The preservation of this equilibrium at the numerical level is not automatic and numerical schemes must be specifically designed in order to balance the discretization of the flux and the source in this situation. Such schemes are often denoted as well-balanced or they are said to enjoy the C-property [6, 9, 18, 20, 26, 4, 31, 32, 33]. These methods increase the accuracy of the solutions when close to these equilibria, but not only. It is possible to see great improvement in their errors also for more general tests.

There are also other types of steady states that solve the shallow water equations. A generalized form of the lake at rest is obtained when the discharge is not zero, but constant in space. In this situation, many equilibria can occur. Again, an analytical solution is not always available, but some implicit forms of the solution [17] are known. It is then interesting to build schemes that are able to preserve also these equilibria at the discrete level.

A class of schemes has been built in the recent years with the aim of preserving such equilibria [11, 10, 12]. They rely on the idea of defining a global flux that incorporates both the flux and the source term thanks to a discretization of the integral of the source term. It is possible to define a numerical scheme that depends only on this global flux and, hence, when reaching the equilibrium the scheme guarantees to preserve the constant global flux at machine precision, including the constant discharge. These techniques not only guarantee the preservation of these equilibria, but also improve the general accuracy of the solution.

In this work, we aim at maximizing the accuracy of simulations by combining the flux globalization technique and the high order accuracy of finite volume methods with WENO reconstructions. We study how a high order reconstruction can be included in the definition of the global flux. A special care is needed in the choice of the discretization of the source term, in particular in the used quadrature formula. Moreover, to exactly preserve the lake-at-rest steady state, a further modification must be done in the definition of the discretized source integral, in order to guarantee the well-balancedness property. The procedure requires a special discretization of the source term and an upwinding technique to compute the numerical flux.

The work is organized as follows. In Section 2 we introduce the shallow water equations and the steady state equilibria that we want to preserve. In Section 3 we introduce the spatial discretization including the finite volume discretization, the global flux definition, the lake-at-rest well-balanced modification and the high order WENO reconstruction. In Section 4 we describe the Deferred Correction method, an arbitrarily high order time integration method. In Section 5 we perform several tests showing the superior capability of the global flux high order method with respect to other high order methods. Finally, in Section 6 we draw some conclusions and we describe some perspective future works.

## 2 Shallow Water Equations

### 2.1 Model

The shallow water equations (SWE) model the behaviour of shallow free surface flows under the action of gravity. They are used to simulate the flows in rivers and coastal areas, and can be applied to predict tides, storm surge levels and coastline changes from hurricanes and ocean currents. They are also used in atmospheric flows, debris flows, and certain hydraulic structures like open channels and sedimentation tanks. SWEs take the form of non-homogeneous hyperbolic conservation laws with source terms modeling the effects of bathymetry and viscous friction. In this paper, we will consider the effect of the bathymetry and the friction as source terms. If the bottom topography is assumed to be constant with respect to time, the SWEs can be recast in balance law form as:

$$\frac{\partial \mathbf{u}}{\partial t} + \frac{\partial \mathcal{F}(\mathbf{u})}{\partial x} = \mathcal{S}(\mathbf{u}, x) \quad \text{on} \quad \Omega_T = \Omega \times [0, T] \subset \mathbb{R} \times \mathbb{R}^+ \quad (1)$$

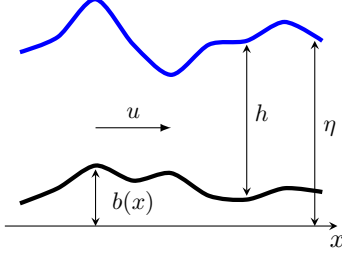


Figure 1: Shallow Water Equations: definition of the variables.

with conserved variables, flux and source term given by

$$\mathbf{u} = \begin{bmatrix} h \\ q \end{bmatrix}, \quad \mathcal{F}(\mathbf{u}) = \begin{bmatrix} q \\ \frac{q^2}{h} + g\frac{h^2}{2} \end{bmatrix}, \quad \mathcal{S}(\mathbf{u}, x) = \begin{bmatrix} 0 \\ S(\mathbf{u}, x) \end{bmatrix} = -gh \begin{bmatrix} 0 \\ \frac{\partial b(x)}{\partial x} \end{bmatrix} - gq \begin{bmatrix} 0 \\ \frac{n^2}{h^{7/3}}|q| \end{bmatrix} \quad (2)$$

where  $h$  represents the relative water height,  $q$  is its discharge (equal to  $hu$ , where  $u$  is the vertically averaged velocity),  $g$  is the gravitational acceleration,  $b(x)$  is the local bathymetry and  $n$  is the Manning friction coefficient. The source term helps modeling the effects induced on the flow caused by the bathymetry changes in space. Finally, it is also convenient to introduce the free surface water level  $\eta := h + b$ . All the aforementioned variables can be better interpreted by looking at Figure 1.

The idea based on global fluxes consists in incorporating the source term in the flux term and rewriting the conservation law (1) in the following equivalent form:

$$\frac{\partial \mathbf{u}}{\partial t} + \frac{\partial \mathcal{G}(\mathbf{u}, x)}{\partial x} = 0 \quad \text{such that} \quad \mathcal{G}(\mathbf{u}, x) = \begin{bmatrix} q \\ K \end{bmatrix} = \begin{bmatrix} q \\ \frac{q^2}{h} + g\frac{h^2}{2} + \mathcal{R} \end{bmatrix} \quad (3)$$

so that  $K$  becomes a global equilibrium variable with

$$\mathcal{R}(x, t) := - \int^x S(\mathbf{u}, \xi) \, d\xi = g \int^x \left[ h(\xi, t) \frac{\partial b(\xi)}{\partial \xi} + \frac{n^2}{h^{7/3}(\xi, t)} |q(\xi, t)| q(\xi, t) \right] \, d\xi \quad (4)$$

System (3) is therefore a hyperbolic system with a global flux, which can be solved with classical techniques for conservation laws without special treatments of the source term. The advantage of the global flux is to have a natural formulation of a quantity  $\mathcal{R}$  that can be balanced for steady state solutions.

## 2.2 Steady state equilibria

As it is described in [9, 8, 28, 37, 43], the construction and development of effective and accurate numerical methods for the shallow water equations have received much interest in the last decades and it is still ongoing. In particular, one is interested in schemes that preserve physical quantities or structures from the continuous level. In this paper, we are addressing two types of difficulties: the preservation of moving steady state equilibria and the preservation of the lake at rest solution.

The SWE system (2) is known to admit some steady state solutions whose form depends on the equilibrium between the source terms  $\mathcal{S}$  and the flux  $\mathcal{F}$  of the equations. The numerical simulations should be able to capture these behaviors even on coarse grids. Without additional techniques, many methods fail at balancing the source terms and the flux, resulting in small perturbations of the steady state. These perturbations could be then amplified by the method causing a bad approximation of the exact behaviour. This phenomenon is sometimes called *numerical storm* in such context. To prevent it, one is interested in schemes that are capable of exactly balancing the flux and the source terms to obtain the desired steady-state solution. Numerical schemes enjoying this property are called **well-balanced (WB) schemes**.

The still water surface is often the first equilibrium taken in consideration. It is given by

$$u = 0; \quad \eta(x, t) = h(x, t) + b(x) \equiv \eta_0 \in \mathbb{R}, \quad \forall x \in \Omega, t \in [0, T]. \quad (5)$$

It represents a steady-state solution, and is referred to as **lake at rest**. However, that is only a special case of the **moving water equilibrium**. The steady state solutions are characterized by the invariants

$$h(x, t)u(x, t) \equiv q_0 \quad \text{and} \quad K(x, t) = \frac{q^2}{h} + g\frac{h^2}{2} + \int_{x_0}^x g \left[ h(\xi, t) \frac{\partial b(\xi)}{\partial \xi} + \frac{n^2}{h^{7/3}(\xi, t)} |q(\xi, t)| q(\xi, t) \right] d\xi \equiv K_0. \quad (6)$$

Obviously, the lake at rest (5) is a special case of (6) when the velocity reduces to zero. Other balanced states can be found in, *inter alia*, [37].

It is interesting [31, 32] to observe that the property (6) in case of smooth solutions and without friction can be rewritten as follows

$$q \equiv q_0, \quad (7)$$

$$0 = \partial_x \left( \frac{q^2}{h} + g\frac{h^2}{2} \right) + gh\partial_x b = -\frac{q_0^2}{h^2} \partial_x h + gh\partial_x h + gh\partial_x b = h\partial_x \left( \frac{q_0^2}{2h^2} + g(h+b) \right). \quad (8)$$

Then, the last equation sum up to verify that  $\Upsilon := \frac{q^2}{2h^2} + g(h+b) \equiv \Upsilon_0$  is constant in space and time. Clearly, this condition does not hold when bathymetry or water height are discontinuous in some points, while (6) is always preserved.

### 3 Space discretization: Global Flux Finite Volume method

The hyperbolic system considered herein is solved by means of the Method Of Lines (MOL). Hence, in this setting, space and time can be treated independently. This section has the goal of presenting a modified arbitrary high order finite volume framework for balance laws with global fluxes. A second order global flux approach is available in [10], but it is limited to linear reconstructions. In this section we aim at building an arbitrary high order global flux method based on WENO reconstructions.

The computational domain  $\Omega$  is discretized into  $N_x$  equispaced control volumes  $\Omega_i = [x_{i-1/2}, x_{i+1/2}]$  of size  $\Delta x$  centered at  $x_i = i\Delta x$  with  $i = i_\ell, \dots, i_r$ .

Considering the system of hyperbolic balance laws described by (1) and (2), for the control volume  $\Omega_i$  we can define the cell average at time  $t$ :

$$\bar{\mathbf{U}}_i(t) := \frac{1}{\Delta x} \int_{x_{i-1/2}}^{x_{i+1/2}} \mathbf{u}(x, t) dx. \quad (9)$$

The semi-discrete central upwind scheme for the system (3) reads

$$\frac{d\bar{\mathbf{U}}_i}{dt} + \frac{1}{\Delta x} (\mathbf{H}_{i+1/2} - \mathbf{H}_{i-1/2}) = 0, \quad (10)$$

where  $\mathbf{H}_{i+1/2}$  is a numerical flux consistent with the global flux  $\mathcal{G}$ . The global flux differs from the original flux and this makes tricky the development of an upwind scheme based on the solution of Riemann problems by an approximate solver. Thus, we are going to employ an upwind scheme that can be easily applied to problems with global fluxes. In order to have a global flux formulation, all the update terms must depend only on the global flux  $\mathcal{G}$  itself. In this way, when we reach a numerical steady state, we are sure that  $\mathcal{G}$  is constant all over the domain. We start from  $\mathcal{G}_i$  cell average values and we reconstruct the global flux at interfaces with a high order WENO procedure. Then, we choose  $\mathbf{H}_{i+1/2}$  to be an upwind numerical flux defined only on the global flux:

$$\mathbf{H}_{i+1/2} = L^{-1} \Lambda^+ L \mathcal{G}_{i+1/2}^L + L^{-1} \Lambda^- L \mathcal{G}_{i+1/2}^R. \quad (11)$$

Here,  $\mathcal{G}_{i+1/2}^{L,R}$  are the discontinuous reconstructed point values of the global flux  $\mathcal{G}(\mathbf{U})$  respectively at the left and right side of the cell interface  $x_{i+1/2}$ .  $L$  is the matrix of the left eigenvectors computed from the flux

Jacobian of the hyperbolic problem (1) in the Roe averaged state, i.e.,

$$J(\mathbf{U}^*) = \begin{pmatrix} 0 & 1 \\ -u_*^2 + gh_* & 2u_* \end{pmatrix}, \quad \text{with } \begin{cases} h_* = \frac{h^L + h^R}{2}, \\ u_* = \frac{\sqrt{h^L} u^L + \sqrt{h^R} u^R}{\sqrt{h^L} + \sqrt{h^R}}. \end{cases} \quad (12)$$

$\Lambda^\pm$  correspond to the upwinding weights

$$\Lambda_i^+ = \begin{cases} 1, & \text{if } \lambda_i > 0, \\ 0, & \text{if } \lambda_i < 0, \end{cases} \quad \Lambda_i^- = \begin{cases} 1, & \text{if } \lambda_i < 0, \\ 0, & \text{if } \lambda_i > 0. \end{cases} \quad (13)$$

It is important to notice that the Jacobian of the flux cannot be directly computed as not all the quantities are available at the interface (we reconstruct only the global flux, not the conserved quantities). Hence, one has to recover the value of  $h$  from the global flux itself. To do so in a positive manner, we use the technique proposed in [10] and reported in Appendix A.

In order to obtain the reconstructed values at the left and right side of interfaces, we will use a high order WENO reconstruction technique that will be explained in Section 3.3, where starting from cell averages, one obtains a nonlinear reconstruction inside a cell. The procedure explained in [10] is not enough to reach arbitrary high order since it approximates (4) using only the midpoint rule. In particular, we will consider piece-wise continuous reconstructions for all the quantities of interests, i.e.,  $h$ ,  $q$ ,  $b$ ,  $\mathcal{R}$ ,  $\mathcal{G}$  and  $K$ . On the other side,  $S$ , being the derivative of  $\mathcal{R}$ , must be defined in a distributional sense. This means that a particular form of  $S$  must be chosen when integrating it to obtain  $\mathcal{R}$  at the interfaces. The details of this procedure will be specified in Section 3.2.

### 3.1 Global flux definitions

Now, to obtain the reconstruction of the global flux at the interfaces, we need, first of all, the values of the global flux at the cell averages, defined as

$$\bar{\mathcal{G}}_i(\mathbf{u}, x) = \bar{\mathcal{F}}_i(\mathbf{u}) + \left[ \begin{matrix} 0 \\ \bar{\mathcal{R}}_i \end{matrix} \right]. \quad (14)$$

We can compute the cell averaged flux evaluating the flux in some high order quadrature points of the cell, through the WENO reconstruction of the conserved variables in the quadrature points, i.e.,

$$\bar{\mathcal{F}}_i(\mathbf{u}) = \sum_q w_q \mathcal{F}(\tilde{\mathbf{u}}(x_{i,q})). \quad (15)$$

For the cell average of the global integral source  $\mathcal{R}$ , we have to perform a reconstruction based on the source terms evaluated, as well, in the quadrature points. Moreover, it will be performed iteratively, from the left boundary of the domain to the right. So that, the cell averages of the integral source can be defined as

$$\bar{\mathcal{R}}_i \approx \sum_q w_q \mathcal{R}_{i,q}. \quad (16)$$

To obtain  $\mathcal{R}$  in the quadrature points, we have to keep in mind its definition as integral of  $S$  (4). So, we can define them using the right interface values of  $\mathcal{R}$ , i.e.,

$$\mathcal{R}_{i,q} = \mathcal{R}_{i-1/2}^R + \int_{x_{i-1/2}^R}^{x_{i,q}} \tilde{S}(x) dx = \mathcal{R}_{i-1/2}^R + \underbrace{\sum_{\theta} \int_{x_{i-1/2}^R}^{x_{i,q}} l_{\theta}(x) dx}_{r_{\theta}^q} S(x_{i,\theta}), \quad (17)$$

where  $\tilde{S}$  is a high order reconstruction of  $S$  done in quadrature points  $x_{i,q}$  for each cell and  $l_{\theta}$  are Lagrangian polynomials in the quadrature points:

$$\tilde{S}_i(x) = \sum_{\theta} l_{\theta}(x) S(x_{i,\theta}). \quad (18)$$

This definition necessitates the values of  $\mathcal{R}$  at the right interface. In order to define a global  $\mathcal{R}$ , we need to define it on both sides of the interfaces. In particular, we can define  $\mathcal{R}$  up to a constant, so we impose that  $\mathcal{R}$  at the left extrema is equal to 0, i.e.,

$$\mathcal{R}_{i_\ell-1/2}^R = 0. \quad (19)$$

Then, we proceed with the integration from left to right, obtaining the values of  $\mathcal{R}$  at the left interfaces from the right interface ones:

$$\mathcal{R}_{i+1/2}^L = \mathcal{R}_{i-1/2}^R + \int_{x_{i-1/2}^R}^{x_{i+1/2}^L} S(\mathbf{u}(x), x) dx = \mathcal{R}_{i-1/2}^R + \Delta x \bar{S}_i, \quad i > i_\ell, \quad (20)$$

with  $\bar{S}_i$  being the cell average of  $S$  computed as

$$\bar{S}_i := \frac{1}{\Delta x} \int_{x_{i-1/2}^R}^{x_{i+1/2}^L} S(\mathbf{u}, \xi) d\xi \approx \sum_q w_q S(x_{i,q}). \quad (21)$$

Finally, we need to give a recursive definition of the right interface values as

$$\mathcal{R}_{i+1/2}^R = \mathcal{R}_{i+1/2}^L + \llbracket \mathcal{R}_{i+1/2} \rrbracket, \quad (22)$$

where  $\llbracket \mathcal{R}_{i+1/2} \rrbracket$  denotes the jump of  $\mathcal{R}$  on  $x_{i+1/2}$ . At this level, we still need to define how we compute the source in the quadrature points  $S(x_{i,\theta})$  and the jump of the integral source  $\llbracket \mathcal{R}_{i+1/2} \rrbracket$ .

Since  $S$  is defined only in a distribution sense, the definition of the jump needs a careful choice. Essentially,  $S$  on the interfaces is a Dirac delta function as we need to compute the derivative of the bathymetry which is discontinuous. The definition of such term in order to have a high order scheme is not uniquely determined. Hence, it will be chosen so that the scheme is consistent and balanced with the flux in the lake at rest equilibrium. In the next section, we describe how to obtain the discretization of the source and of the jump of the integral of the source.

### 3.2 Global Flux formulation for lake at rest preservation

By construction, the scheme presented so far is able to preserve a constant global flux for the family of moving equilibria solutions, i.e.,  $q \equiv q_0$  and  $K \equiv K_0$ . However, in the lake at rest simulation, the preservation of the constant water free surface does not come for free, in particular we cannot preserve *a priori*  $\eta = h + b \equiv \eta_0$ . Therefore, a special treatment of the source term is required to assure so. The friction term is neglected here, because it vanishes when the speed is zero as in the lake at rest equilibrium.

We start defining a high order reconstruction of  $h$ ,  $\eta$  and  $b$  in a cell  $\Omega_i$  using the WENO reconstruction with the same weights for  $h$ ,  $\eta$  and  $b$ . In particular, the weights will be chosen according to  $\eta$  in order to preserve the lake at rest balance. This means that we obtain a reconstructions for the three variables in the quadrature points  $x_{i,q}$  that we denote with  $\tilde{h}_{i,q}$ ,  $\tilde{\eta}_{i,q}$  and  $\tilde{b}_{i,q}$ , and they are such that

$$\tilde{h}_{i,q} = \tilde{\eta}_{i,q} - \tilde{b}_{i,q}. \quad (23)$$

We start by recasting the source term, given that  $h(x) = \eta(x) - b(x)$ ,

$$S(\mathbf{u}, x) = gh(x)\partial_x b(x) = g\eta(x)\partial_x b(x) - g\partial_x \left( \frac{b^2(x)}{2} \right). \quad (24)$$

Equation (24) allows us to give proper shape to (20), which now reads

$$\mathcal{R}_{i+1/2}^L = \mathcal{R}_{i-1/2}^R - \int_{x_{i-1/2}^R}^{x_{i+1/2}^L} S(\mathbf{u}(x), x) dx \quad (25)$$

$$= \mathcal{R}_{i-1/2}^R + g \int_{x_{i-1/2}^R}^{x_{i+1/2}^L} \eta(x) \partial_x b(x) dx - g \left( \frac{(b_{i+1/2}^L)^2}{2} - \frac{(b_{i-1/2}^R)^2}{2} \right) \quad (26)$$

$$(\text{if } \eta \equiv \eta_0) = \mathcal{R}_{i-1/2}^R + g\eta_0 (b_{i+1/2}^L - b_{i-1/2}^R) - g \left( \frac{(b_{i+1/2}^L)^2}{2} - \frac{(b_{i-1/2}^R)^2}{2} \right). \quad (27)$$

As we see, the values of the bathymetry at the interfaces of the cells are necessary to compute (25). It is crucial to maintain the well balanced structure in the quadrature points  $x_{i,q}$ , hence, we reconstruct  $b_{i+1/2}^L$  and  $b_{i-1/2}^R$  using a Lagrangian polynomial interpolating the values at the quadrature points, i.e.,

$$\tilde{b}_i(x) := \sum_q \ell_q(x) \tilde{b}_{i,q}, \quad \text{and} \quad b_{i+1/2}^L = \tilde{b}_i(x_{i+1/2}), \quad b_{i-1/2}^R = \tilde{b}_i(x_{i-1/2}). \quad (28)$$

Equation (27), corresponding to the case  $\eta \equiv \eta_0$ , is the value that  $\mathcal{R}_{i+1/2}^L$  assumes at the interface when the lake at rest is preserved. However, to get there, a proper discretization of the integral  $\int_{x_{i-1/2}^R}^{x_{i+1/2}^L} \eta(x) \partial_x b(x)$  should be performed. To do so, let us introduce  $Q(x) := g\eta(x) \partial_x b(x)$  and let us reconstruct it as the source term in (18) and we can integrate it using ad hoc quadrature formulae.

$$\int_{x_{i-1/2}^R}^{x_{i+1/2}^L} \tilde{Q}(x) dx = \int_{x_{i-1/2}^R}^{x_{i+1/2}^L} \sum_{\theta} \ell_{\theta}(x) dx Q_{i,\theta}, \quad (29)$$

where

$$Q_{i,\theta} = \tilde{\eta}_{i,\theta} \sum_q \ell'_q(x_{i,\theta}) \tilde{b}_{i,q}. \quad (30)$$

In particular, we applied the same approach to treat the derivative of the bathymetry. The fully integrated relation for  $\mathcal{R}_{i+1/2}^L$  now becomes

$$\mathcal{R}_{i+1/2}^L = \mathcal{R}_{i-1/2}^R + \int_{x_{i-1/2}^R}^{x_{i+1/2}^L} \sum_{\theta} \ell_{\theta}(x) dx Q_{i,\theta} - g \left( \frac{(b_{i+1/2}^L)^2}{2} - \frac{(b_{i-1/2}^R)^2}{2} \right) \quad (31)$$

$$= \mathcal{R}_{i-1/2}^R + g \sum_{\theta} \int_{x_{i-1/2}^R}^{x_{i+1/2}^L} \ell_{\theta}(x) dx \tilde{\eta}_{i,\theta} \sum_s \ell'_s(x_{\theta}) \tilde{b}_{i,s} - g \left( \frac{(b_{i+1/2}^L)^2}{2} - \frac{(b_{i-1/2}^R)^2}{2} \right). \quad (32)$$

Notice that the value of the bathymetry at the interfaces and the derivative of the bathymetry in the quadrature points is given by the same reconstruction (28). So, when  $\eta \equiv \eta_0$ , we have that

$$\begin{aligned} \mathcal{R}_{i+1/2}^L &= \mathcal{R}_{i-1/2}^R + g\eta_0 \int_{x_{i-1/2}^R}^{x_{i+1/2}^L} \sum_s \tilde{b}_{i,s} \ell'_s(x) dx - g \left( \frac{(b_{i+1/2}^L)^2}{2} - \frac{(b_{i-1/2}^R)^2}{2} \right) \\ &= \mathcal{R}_{i-1/2}^R + g\eta_0 (b_{i+1/2}^L - b_{i-1/2}^R) - g \left( \frac{(b_{i+1/2}^L)^2}{2} - \frac{(b_{i-1/2}^R)^2}{2} \right). \end{aligned} \quad (33)$$

Following the same reasoning  $\mathcal{R}_{i,q}$  introduced in (17) can be recast as

$$\mathcal{R}_{i,q} = \mathcal{R}_{i-1/2}^R - \int_{x_{i-1/2}^R}^{x_{i,q}} S(\mathbf{u}(x), x) dx \quad (34)$$

$$= \mathcal{R}_{i-1/2}^R + g \int_{x_{i-1/2}^R}^{x_{i,q}} \eta(x) \partial_x b(x) dx - g \left( \frac{(b_{i,q})^2}{2} - \frac{(b_{i-1/2}^R)^2}{2} \right) \quad (35)$$

$$(\text{if } \eta \equiv \eta_0) = \mathcal{R}_{i-1/2}^R + g\eta_0 (b_{i,q} - b_{i-1/2}^R) - g \left( \frac{(b_{i,q})^2}{2} - \frac{(b_{i-1/2}^R)^2}{2} \right). \quad (36)$$

Once again, this last identity corresponds to the solution at the lake at rest condition but the integral  $\int_{x_{i-1/2}^R}^{x_{i,q}} \eta(x) \partial_x b(x) dx$  has to be discretized to be consistent also for other solutions. Following what we did in (25), (34) becomes

$$\mathcal{R}_{i,q} = \mathcal{R}_{i-1/2}^R - \int_{x_{i-1/2}^R}^{x_{i,q}} \tilde{S}(x) dx \quad (37)$$

$$= \mathcal{R}_{i-1/2}^R + \sum_{\theta} \int_{x_{i-1/2}^R}^{x_{i,q}} \ell_{\theta}(x) dx \tilde{Q}_{i,\theta} - g \left( \frac{(b_{i,q})^2}{2} - \frac{(b_{i-1/2}^R)^2}{2} \right) \quad (38)$$

$$= \mathcal{R}_{i-1/2}^R + g \sum_{\theta} \int_{x_{i-1/2}^R}^{x_{i,q}} \ell_{\theta}(x) dx \tilde{\eta}_{i,\theta} \sum_s \ell'_s(x_{i,\theta}) \tilde{b}_{i,s} - g \left( \frac{(b_{i,q})^2}{2} - \frac{(b_{i-1/2}^R)^2}{2} \right). \quad (39)$$

So that, when  $\eta \equiv \eta_0$ , we have

$$\mathcal{R}_{i,q} = \mathcal{R}_{i-1/2}^R + g\eta_0 \int_{x_{i-1/2}^R}^{x_{i,q}} \sum_s \ell'_s(x_{i,\theta}) \tilde{b}_{i,s} dx \tilde{\eta}_{i,\theta} - g \left( \frac{(b_{i,q})^2}{2} - \frac{(b_{i-1/2}^R)^2}{2} \right) \quad (40)$$

$$= \mathcal{R}_{i-1/2}^R + g\eta_0 (\tilde{b}_{i,q} - b_{i-1/2}^R) - g \left( \frac{(b_{i,q})^2}{2} - \frac{(b_{i-1/2}^R)^2}{2} \right). \quad (41)$$

We still have not defined the jump of the integral source term  $[\mathcal{R}_{i+1/2}]$ . Equipped with (25) and (34), considering  $\eta \equiv \eta_0$  and  $q \equiv 0$ , we can build it such that the cell averages  $\bar{K}_i$  are constant in all the cells. We have that

$$K_{i,q} = \mathcal{F}_{i,q} + \mathcal{R}_{i,q} = \mathcal{R}_{i-1/2}^R + g \frac{(\eta_0 - b_{i,q})^2}{2} + g\eta_0 (b_{i,q} - b_{i-1/2}^R) - g \left( \frac{(b_{i,q})^2}{2} - \frac{(b_{i-1/2}^R)^2}{2} \right) \quad (42)$$

$$= \mathcal{R}_{i-1/2}^R + g \frac{\eta_0^2}{2} - g\eta_0 b_{i,q} + g \frac{b_{i,q}^2}{2} + g\eta_0 (b_{i,q} - b_{i-1/2}^R) - g \left( \frac{(b_{i,q})^2}{2} - \frac{(b_{i-1/2}^R)^2}{2} \right) \quad (43)$$

$$= \mathcal{R}_{i-1/2}^R + g \frac{\eta_0^2}{2} - g\eta_0 b_{i-1/2}^R + g \frac{(b_{i-1/2}^R)^2}{2} \quad (44)$$

and, clearly,  $\bar{K}_i = K_{i,q}$  for all  $q$ . Hence, to prove that the scheme is indeed well-balanced for the lake at rest solution, we set  $\bar{K}_{i+1} - \bar{K}_i = 0$ :

$$\bar{K}_{i+1} - \bar{K}_i = \mathcal{R}_{i+1/2}^R - \mathcal{R}_{i-1/2}^R - g\eta_0 b_{i+1/2}^R + g \frac{(b_{i+1/2}^R)^2}{2} + g\eta_0 b_{i-1/2}^R - g \frac{(b_{i-1/2}^R)^2}{2} \stackrel{!}{=} 0. \quad (45)$$

Now we compute the differences of the integral sources using (33) and we get

$$\mathcal{R}_{i+1/2}^R - \mathcal{R}_{i-1/2}^R = \mathcal{R}_{i+1/2}^L - \mathcal{R}_{i-1/2}^R + [\mathcal{R}_{i+1/2}] \quad (46)$$

$$= g\eta_0 (b_{i+1/2}^L - b_{i-1/2}^R) - g \left( \frac{(b_{i+1/2}^L)^2}{2} - \frac{(b_{i-1/2}^R)^2}{2} \right) + [\mathcal{R}_{i+1/2}]. \quad (47)$$



Inserting (46) in (45), we get

$$\bar{K}_{i+1} - \bar{K}_i = g\eta_0 \left( b_{i+1/2}^L - b_{i-1/2}^R \right) - g \left( \frac{(b_{i+1/2}^L)^2}{2} - \frac{(b_{i-1/2}^R)^2}{2} \right) + \llbracket \mathcal{R}_{i+1/2} \rrbracket \quad (48)$$

$$-g\eta_0 b_{i+1/2}^R + g \frac{(b_{i+1/2}^R)^2}{2} + g\eta_0 b_{i-1/2}^L - g \frac{(b_{i-1/2}^L)^2}{2} \stackrel{!}{=} 0, \quad (49)$$

which is indeed equal to zero if

$$\llbracket \mathcal{R}_{i+1/2} \rrbracket \stackrel{!}{=} g\eta_0 \left( b_{i+1/2}^R - b_{i+1/2}^L \right) - g \left( \frac{(b_{i+1/2}^R)^2}{2} - \frac{(b_{i+1/2}^L)^2}{2} \right).$$

In order to have a consistent approximation of the jump of the integral source  $\llbracket \mathcal{R}_{i+1/2} \rrbracket$ , we define it as

$$\llbracket \mathcal{R}_{i+1/2} \rrbracket := g \frac{\eta_{i+1/2}^R + \eta_{i+1/2}^L}{2} \left( b_{i+1/2}^R - b_{i+1/2}^L \right) - g \left( \frac{(b_{i+1/2}^R)^2}{2} - \frac{(b_{i+1/2}^L)^2}{2} \right). \quad (50)$$

**Remark 3.1** (Friction). *When adding the friction term to the global flux, we do not need to be so careful. Indeed, the friction term is defined as rational of polynomials of conservative variables that can be reconstructed piecewise continuously on the mesh. Hence, they do not contribute to the jump of  $\mathcal{R}$  at the interfaces. So, it is enough to define*

$$\mathcal{R}_{i,q} := \mathcal{R}_{i-1/2}^R + g \sum_{\theta} \int_{x_{i-1/2}^R}^{x_{i,q}} \ell_{\theta}(x) \, dx \left( \tilde{\eta}_{i,\theta} \sum_s \ell'_s(x_{i,\theta}) \tilde{b}_{i,s} + g \frac{\tilde{q}_{i,\theta} |\tilde{q}_{i,\theta}| n^2}{\tilde{h}_{i,\theta}^{7/3}} \right) - g \left( \frac{(b_{i,q})^2}{2} - \frac{(b_{i-1/2}^R)^2}{2} \right) \quad (51)$$

and

$$\mathcal{R}_{i+1/2}^L := \mathcal{R}_{i-1/2}^R + g \sum_{\theta} \int_{x_{i-1/2}^R}^{x_{i+1/2}} \ell_{\theta}(x) \, dx \left( \tilde{\eta}_{i,\theta} \sum_s \ell'_s(x_{i,\theta}) \tilde{b}_{i,s} + g \frac{\tilde{q}_{i,\theta} |\tilde{q}_{i,\theta}| n^2}{\tilde{h}_{i,\theta}^{7/3}} \right) - g \left( \frac{(b_{i+1/2}^L)^2}{2} - \frac{(b_{i-1/2}^R)^2}{2} \right). \quad (52)$$

In Algorithm 1 we summarize the steps of the reconstruction of the source integral.

---

**Algorithm 1** Source integral reconstruction

---

$\mathcal{R}_{i_{l-1/2}} := 0$

**for**  $i = i_l, \dots, i_r$  **do**

Reconstruct the variables  $h$ ,  $\eta$  and  $b$  in the quadrature point of the cell, obtaining  $\tilde{h}_{i,\theta}$ ,  $\tilde{\eta}_{i,\theta}$  and  $\tilde{b}_{i,\theta}$  with the same weights

Reconstruct  $q$  in the quadrature points obtaining  $\tilde{q}_{i,\theta}$

Define  $\mathcal{R}_{i,q}$  as in (51)

Define  $\mathcal{R}_{i+1/2}^L$  as in (52)

Define  $\llbracket \mathcal{R}_{i+1/2} \rrbracket$  as in (50)

Define  $\mathcal{R}_{i+1/2}^R := \mathcal{R}_{i+1/2}^L + \llbracket \mathcal{R}_{i+1/2} \rrbracket$

**end for**

---

### 3.3 Weighted Essentially Non-Oscillatory (WENO) method

#### 3.3.1 Scalar reconstruction

The WENO method is a high order accurate reconstruction of the solution at some prescribed points. In particular, we are interested in finding the value of the solution at cell interfaces  $x_{i+1/2}$  given the cell averages

of the solutions in the neighboring cells. We will denote the high order accurate reconstructed variables as  $u_{i+1/2}^L$  and  $u_{i+1/2}^R$  at the left and the right side of the interface, respectively. The left value is obtained by reconstructing the variable in  $\Omega_i$ , while the right value is recovered performing the same reconstruction in  $\Omega_{i+1}$ . In order to obtain a high order  $p$  reconstruction, with  $p$  odd, we consider  $p$  cells that constitute a stencil:

$$\{\Omega_{l_x}, \quad l_x = i - r + 1, \dots, i + r - 1\}, \quad (53)$$

where  $2r - 1 = p$ . As an example, WENO reconstruction with order 5 (WENO5) will use a stencil of length  $p = 5$  with  $r = 3$  low order reconstructions. The involved cells are from  $i - 2$  to  $i + 2$ .

In practice WENO considers a high order reconstruction polynomials  $p^{HO}$  that fulfills all the constraints

$$\frac{1}{\Delta x} \int_{x_{i-j-1/2}}^{x_{i-j+1/2}} p^{HO}(x) dx = u_{i-j}, \quad j = -r + 1, \dots, r - 1, \quad (54)$$

and  $r$  low order  $(r - 1)$  polynomials  $p_m(x)$   $m = 0, \dots, r - 1$  that fulfill

$$\frac{1}{\Delta x} \int_{x_{i-r+j+m-1/2}}^{x_{i-r+j+m+1/2}} p_m(x) dx = u_{i-j+m}, \quad j = 1, \dots, r. \quad (55)$$

The WENO reconstruction aims at combining the low order polynomials in order to obtain the high order reconstruction in case all the low order polynomials are non-oscillatory, while it will prefer the least oscillatory polynomial in case some of these polynomials show oscillations.

In order to achieve the high order accuracy ( $p$ ), for every quadrature point or flux point  $\xi$  in which we want to reconstruct the polynomial, we look for some optimal weights  $d_m$  such that  $\sum_m d_m p_m(\xi) = p^{HO}(\xi)$ . However, these optimal weights are not enough to control oscillations and Gibbs phenomena, since ‘‘Linear numerical schemes for solving PDEs, having the property of not generating new extrema (monotone scheme), can be at most first-order accurate’’ [21]. Hence, we weigh these optimal weights by

$$\alpha_m = \frac{d_m}{(\beta_m + \epsilon)^2}, \quad \omega_m = \frac{\alpha_m}{\sum_{k=0}^{r-1} \alpha_k}, \quad m = 0, \dots, r - 1, \quad (56)$$

where  $\epsilon$  is needed to avoid division by 0 ( $10^{-30}$  in the simulations) and  $\beta_m$  are the smoothness indicator defined by

$$\beta_m = \sum_{k=1}^{r-1} \int_{x_{i-1/2}}^{x_{i+1/2}} \left( \frac{d^k}{dx^k} p_m(x) \right)^2 \Delta x^{2k-1} dx, \quad m = 0, \dots, r - 1. \quad (57)$$

In this way, we obtain the WENO weights  $\omega_m(\xi)$  that gives the reconstruction in a specific point  $\xi$ :

$$\tilde{u}(\xi) = \sum_{m=0}^{r-1} \omega_m(\xi) p_m(\xi). \quad (58)$$

The values of the optimal weights  $d_m$  and the formulae for computing  $\beta_m$  can be found in [24, 7] up to  $r = 6$ . In the following, we will test the reconstruction with orders  $p = 3$  and  $p = 5$ .

## 4 Time discretization

After the description of the space discretization, we will introduce an arbitrarily high order time integration method. We use the MOL splitting of spatial and time discretization, so we can describe the time discretization for the semidiscretized ODE resulting after the spatial discretization. We will use the Deferred Correction (DeC) method [15, 19, 34] as described in [1, 3, 42, 23]. The DeC is a family of one step methods with arbitrarily high order of accuracy.

## 4.1 Deferred Correction method

The original DeC formulation was introduced in [15], then developed and studied in its different forms in [19, 34, 13, 27], while a slightly different form was presented in [1] with applications to finite element methods. In [1], the DeC is presented as an iterative procedure that involves two operators. The iteration process mimic the Picard–Lindelöf proof at the discrete level with a fixed-point iterative method. At each iteration of this process one order of accuracy is gained and after a finite amount of iterations the aimed accuracy is reached. Let us consider the initial value problem

$$y'(t) = f(y(t)), \quad y(t_0) = y_0, \quad (59)$$

where  $y : \mathbb{R} \rightarrow \mathbb{R}^S$  and  $f : \mathbb{R}^S \rightarrow \mathbb{R}^S$ , where  $f$  can be the semidiscretized operator presented above. The first operator we introduce is  $\mathcal{L}^1$ , a low order approximation of the integral version of the ODE (59) and the solution of  $\mathcal{L}^1(y) = 0$  is easy to obtain, e.g. explicit Euler method. The second operator,  $\mathcal{L}^2$ , is a high order discretization of the ODE and the solution of  $\mathcal{L}^2(y) = 0$  might be difficult to obtain, as an implicit RK method. The DeC procedure combines the two operators exploiting the accuracy of  $\mathcal{L}^2$  and the simplicity of  $\mathcal{L}^1$  obtaining an explicit (or easy-to-solve) high order method.

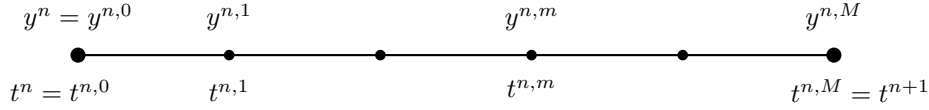


Figure 2: Time interval divided into sub-time steps

Consider a time step  $[t^n, t^{n+1}]$  and let us subdivide it into  $M$  sub-time steps  $\{[t^{n,m-1}, t^{n,m}]\}_{m=1}^M$  where the boundary points coincide with the extrema of the time step, i.e.,  $t^n = t^{n,0}$  and  $t^{n,M} = t^{n+1}$ . We consider a discretization of the variables in the sub-time nodes  $t^{n,m}$  denoted as  $y^{n,m}$  as explained in Figure 2.

We define the  $\mathcal{L}^2$  operator as

$$\mathcal{L}^2(y^{n,0}, \dots, y^{n,M}) := \begin{cases} y^{n,M} - y^{n,0} - \Delta t \sum_{r=0}^M \theta_r^M f(y^{n,r}), \\ \vdots \\ y^{n,1} - y^{n,0} - \Delta t \sum_{r=0}^M \theta_r^1 f(y^{n,r}), \end{cases} \approx \begin{cases} y^{n,M} - y^{n,0} - \int_{t^{n,0}}^{t^{n,M}} f(y(s)) ds, \\ \vdots \\ y^{n,1} - y^{n,0} - \int_{t^{n,0}}^{t^{n,1}} f(y(s)) ds, \end{cases} \quad (60)$$

where  $\theta_r^m$  is the integral of the  $r$ -th Lagrangian basis function defined on the sub-time nodes over the interval  $[t^{n,0}, t^{n,m}]$  [23, 1] normalized by the factor  $\Delta t$ . This operator is a high order discretization of the integral form of the ODE in each sub-time step. Depending on the chosen sub-time nodes, the order of accuracy varies, for example, with equispaced nodes we can obtain a scheme with order  $M + 1$ , while with Gauss-Lobatto nodes we obtain a  $2M$ -th accurate scheme, i.e., the Lobatto IIIA schemes [22]. The system of equations  $\mathcal{L}^2 = 0$  is a (possibly) nonlinear system of equations which might be very complicated to solve as  $f$  is, in our case, the semidiscretization of a nonlinear PDE.

That is why we introduce  $\mathcal{L}^1$  a simplification of the  $\mathcal{L}^2$  operator. The  $\mathcal{L}^1$  operator in this context consists in a explicit Euler discretization in each sub-time step, written as

$$\mathcal{L}^1(y^{n,0}, \dots, y^{n,M}) := \begin{cases} y^{n,M} - y^{n,0} - \beta^M \Delta t f(y^{n,0}), \\ \vdots \\ y^{n,1} - y^{n,0} - \beta^1 \Delta t f(y^{n,0}), \end{cases} \quad (61)$$

where  $\beta^m = \frac{t^{n,m} - t^{n,0}}{\Delta t}$ . The solution of  $\mathcal{L}^1 = 0$  is straightforward.

To simplify the notation of the DeC iterative process, we define a vector of all the variables  $y$  at each sub-time node (we omit the superscript  $n$  as we will always refer to the time step  $[t^n, t^{n+1}]$ ):

$$\mathbf{y} := (y^{n,0}, \dots, y^{n,M}) \in \mathbb{R}^{M \times S}, \text{ such that} \quad (62)$$

$$\mathcal{L}^1(\mathbf{y}) := \mathcal{L}^1(y^{n,0}, \dots, y^{n,M}) \text{ and } \mathcal{L}^2(\mathbf{y}) := \mathcal{L}^2(y^{n,0}, \dots, y^{n,M}). \quad (63)$$

Finally we can introduce the iterations of the DeC algorithm. The aim is to approximate the solution of the  $\mathcal{L}^2$  operator  $\mathbf{y}^*$ , i.e.,  $\mathcal{L}^2(\mathbf{y}^*) = 0$ , with successive iterations, where, at each iteration, we gain one order of accuracy. Let us denote the iterations with the superscript  $(k)$  for  $k = 0, \dots, K$ , so that each variable  $\mathbf{y}^{(k)} \in \mathbb{R}^{(M+1) \times S}$  is composed by the entries  $y^{n,m,(k)} \in \mathbb{R}^S$  with  $m = 0, \dots, M$ .

The DeC algorithm reads

### DeC Algorithm

$$\begin{aligned} y^{n,0,(k)} &:= y(t^n), \quad k = 0, \dots, K, \\ y^{n,m,(0)} &:= y(t^n), \quad m = 1, \dots, M, \\ \mathcal{L}^1(\mathbf{y}^{(k)}) &= \mathcal{L}^1(\mathbf{y}^{(k-1)}) - \mathcal{L}^2(\mathbf{y}^{(k-1)}) \text{ with } k = 1, \dots, K, \end{aligned} \tag{64}$$

where  $K$  is the number of iterations that we want to compute. In particular, after  $K$  iterations the order of accuracy of the method will be the minimum between  $K$  and the accuracy of  $\mathcal{L}^2$ . As an example, to obtain order 5, we need  $K = 5$  and for equispaced sub-time nodes  $M = 4$  (for Gauss–Lobatto  $M = 3$  suffices). A more explicit formulation of iteration step of (64) is the following

$$y^{n,m,(k)} - y^{n,0} - \Delta t \sum_{r=0}^M \theta_r^m f(y^{n,r,(k-1)}) = 0. \tag{65}$$

More details, proofs and properties of the DeC can be found in [23, 2, 42] and references therein.

## 5 Numerical Simulations

The arbitrary high order well-balanced WENO finite volume scheme based on Flux Globalization has been tested and validated on several test cases to assess convergence properties and performances. In Section 5.1 we study the lake at rest steady state case to verify the well-balancedness of the scheme. In Section 5.2 we add a perturbation to the previous tests to compare the quality of well-balanced schemes and not well-balanced ones. In Section 5.3 we focus on more general steady state with nonzero global fluxes and we test the method on subcritical, supercritical and transcritical flows. Finally, in Section 5.4 we add also the friction to the previous tests.

For smooth tests we will perform a convergence analysis to assess the order of accuracy of our methods. In particular, we will validate the algorithm with WENO3 and WENO5 reconstructions.

### 5.1 Lake at rest

Firstly, we consider the lake at rest solution characterized by the initial data

$$h(x, 0) = 1 - b(x), \quad q(x, 0) \equiv 0 \tag{66}$$

over the computational domain  $[0, 25]$  with subcritical inlet/outlet at the two boundaries. The bathymetry employed contains a sinusoidal bump damped at the boundaries (see Figure 3 for better visualization of solution and bathymetry) and it reads

$$b(x) = 0.05 \sin(x - 12.5) \exp(1 - (x - 12.5)^2). \tag{67}$$

Let us remark that the classical bathymetry provided in [17] for many tests is only piecewise polynomial, but globally only  $\mathcal{C}^0$ . Hence, it is not suited to test the accuracy of very high order methods. On the other side, the bathymetry (67) is  $\mathcal{C}^\infty$  and it has values smaller than machine precision at the boundaries. The gravitational constant is considered to be  $g = 1$  and the simulation is run until the final time  $T = 1$  with  $N_e = \{25, 50, 100, 150, 200, 400, 800\}$  uniform cells using both the non-well-balanced (non-WB) and

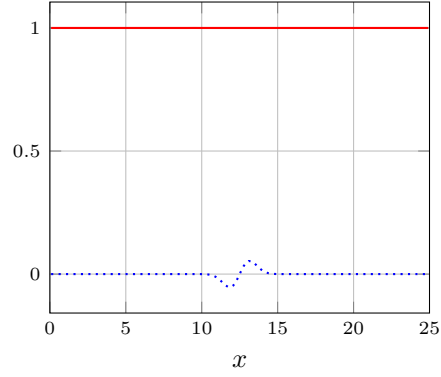


Figure 3: Lake at rest solution:  $\eta$  (red) and  $b$  (blue).

Table 1: Lake at rest: errors and estimated order of accuracy (EOA) with WB and non-WB schemes and WENO3 and WENO5 reconstructions.

$N_e$	Non-WB				WB			
	$h$		$q$		$h$		$q$	
	$L_2$ error	EOA	$L_2$ error	EOA	$L_2$ error	EOA	$L_2$ error	EOA
	GF-WENO3				GF-WENO3			
25	1.0384E-4	–	4.7943E-5	–	9.8858E-14	–	1.2228E-15	–
50	1.5496E-5	2.67	9.2488E-6	2.31	9.8667E-14	–	1.4249E-15	–
100	1.2117E-6	3.62	3.6777E-7	4.59	9.8276E-14	–	1.6041E-15	–
150	2.6776E-7	3.69	1.5898E-7	2.05	1.9644E-13	–	3.3908E-15	–
200	9.6323E-8	3.53	7.6469E-8	2.53	1.9619E-13	–	3.6713E-15	–
400	8.2671E-9	3.53	6.0441E-9	3.65	2.9360E-13	–	6.1689E-15	–
800	6.8811E-10	3.58	4.7122E-10	3.67	5.8655E-13	–	1.3035E-14	–
	GF-WENO5				GF-WENO5			
25	5.1800E-5	–	6.1657E-5	–	9.8947E-14	–	1.3247E-15	–
50	4.4066E-6	3.45	1.5244E-6	5.18	9.8661E-14	–	1.4060E-15	–
100	6.7998E-7	2.66	3.5908E-7	2.06	9.8289E-14	–	1.5992E-15	–
150	1.5437E-7	3.63	8.8535E-8	3.42	1.9639E-13	–	3.4157E-15	–
200	4.1973E-8	4.50	2.3725E-8	4.55	1.9611E-13	–	3.7034E-15	–
400	1.3952E-9	4.89	7.5991E-10	4.95	2.9357E-13	–	6.2007E-15	–
800	4.3120E-11	5.01	2.2633E-11	5.06	5.8648E-13	–	1.3039E-14	–

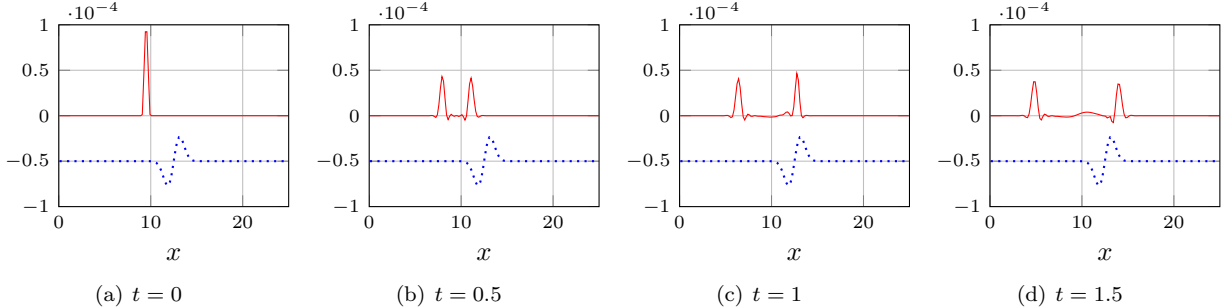


Figure 4: Small perturbation of the lake at rest solution computed with the GF-WENO5 WB scheme:  $h - h_{eq}$  (red) and rescaled  $b$  (blue).

well-balanced (WB) version of the algorithm to assess the convergence and well-balancing properties. The convergence tests performed with WENO3 and WENO5 are listed in Table 1. It can be noticed that the error decay for the non-WB simulations matches the order of the reconstruction for both WENO3 and WENO5, while, for the WB cases, the scheme is able to preserve the exact solution up to machine precision.

## 5.2 Small perturbation of the lake at rest solution

For this test case, we analyze the perturbation of the lake at rest solution characterized by

$$h(x, 0) = 1 - b(x) + \begin{cases} 10^{-5}, & \text{if } 9 < x < 10 \\ 0, & \text{otherwise} \end{cases}, \quad q(x, 0) \equiv 0 \quad (68)$$

over the computational domain  $[0, 25]$  with subcritical inlet/outlet at the two boundaries. The bathymetry is a rescaling of (67) and it is defined as

$$b(x) = 0.5 \sin(x - 12.5) \exp(1 - (x - 12.5)^2). \quad (69)$$

A slightly different bathymetry, with respect to Section 5.1, has been chosen in order to introduce more noise in the non-WB simulation and appreciate more the method capabilities. The simulation was run using a mesh with 150 cells. Figure 4 shows the evolution over time of the perturbation added over the lake at rest solution computed with the GF-WENO5 WB scheme. To better present the results, the plots show the relative variable  $h - h_{eq}$  where  $h_{eq}$  represents the lake at rest solution without perturbation provided in Equation (66). We then compare the results in Figure 4 with those computed using the classical WENO5 approach, pointed out in Figure 5. It should be noticed that the classical approach fails at correctly reproducing the perturbation. Indeed, it generates a discretization error of several orders of magnitude higher than the perturbation itself, eventually spoiling the final result. Contrary to that, the GF-WENO5 WB scheme correctly reproduce the perturbation which splits into two waves traveling at opposite directions and interacting with the bathymetry. The obtained result is fairly accurate, also considering the coarse mesh used for this study.

## 5.3 Steady states without friction ( $n = 0$ )

Here, we test the method for some moving equilibria steady state problems. We run the tests up to convergence towards steady state in different situations. In the subcritical and supercritical tests the bathymetry is smooth and equal to (67), as we want to assess the high order accuracy of the schemes. For the transcritical tests we use a modification of the bathymetry used in [17], to study a very similar discontinuous problem. Depending on the initial and boundary conditions set at the borders of the domain, the flow may be supercritical, subcritical or transcritical. The meshes used are with  $N_e \in \{25, 50, 75, 100, 125, 150, 250, 500\}$ . We consider the following three sets of initial and boundary conditions:

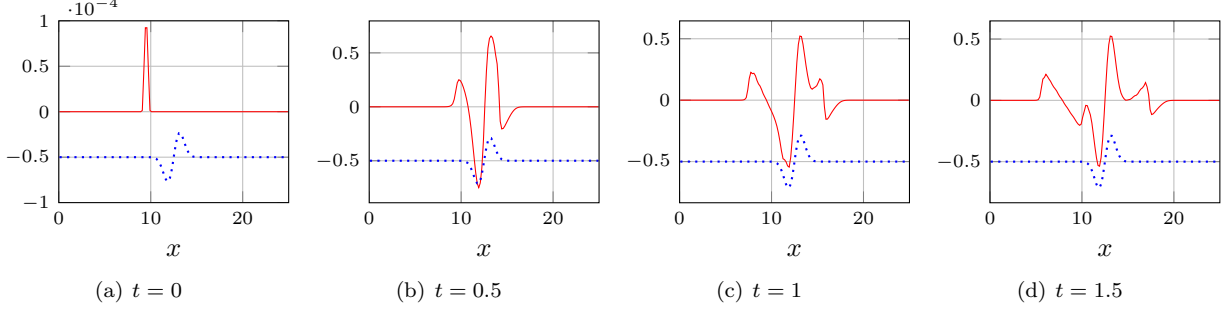


Figure 5: Small perturbation of the lake at rest solution computed with the WENO5 scheme:  $h - h_{eq}$  (red) and rescaled  $b$  (blue).

- Supercritical flow

$$\begin{aligned} h(x, 0) &= 2 - b(x), & q(x, 0) &\equiv 0, \\ h(0, t) &= 2, & q(0, t) &= 24, \end{aligned} \quad (70)$$

- Subcritical flow

$$\begin{aligned} h(x, 0) &= 2 - b(x), & q(x, 0) &\equiv 0, \\ q(0, t) &= 4.42, & h(25, t) &= 2, \end{aligned} \quad (71)$$

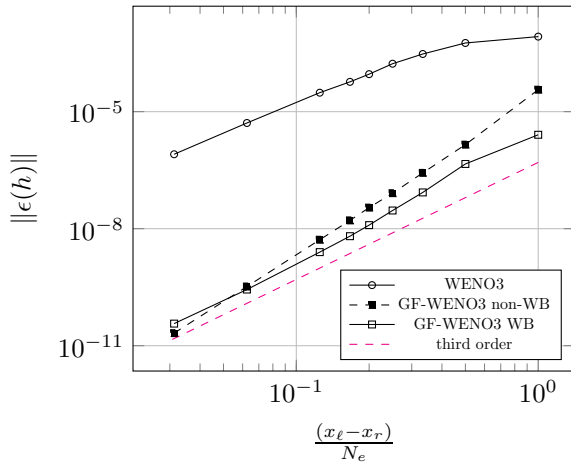
- Transcritical flow

$$\begin{aligned} b(x) &= \begin{cases} 0.2 \exp\left(1 - \frac{1}{1 - \left(\frac{|x-10|}{5}\right)^2}\right), & \text{if } |x - 10| < 5, \\ 0, & \text{else,} \end{cases} \\ h(x, 0) &= 0.33 - b(x), & q(x, 0) &\equiv 0, \\ q(0, t) &= 0.18, & h(25, t) &= 0.33. \end{aligned} \quad (72)$$

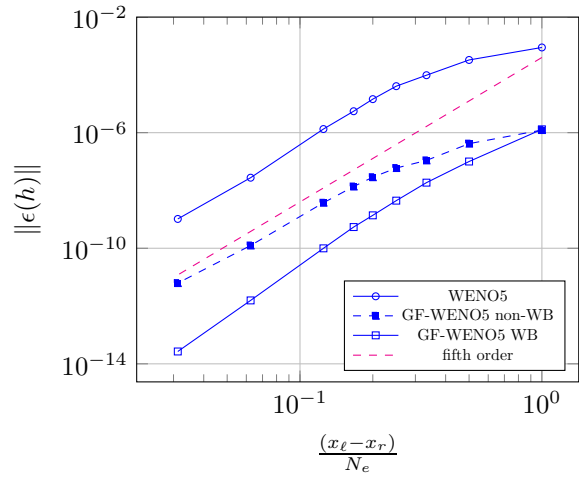
The gravitational constant is set to  $g = 9.812$  for all these tests. For these three cases, we compare the results obtained using a classical WENO finite volume scheme and the new approach based on flux globalization. As already mentioned, for supercritical and subcritical cases, the bathymetry (67) allows us to perform convergence tests for very high order methods, when also the flow is smooth. For the transcritical case with shock, only a qualitative analysis of the test is performed. Hence, when supercritical and subcritical flows are of interest, we can study the convergence properties of the new scheme by finding the exact solution given by the non-linear equations taken from [17]. Both the WB and non-WB versions of the scheme have been run to compare the influence of the formulation on the ability of preserving the balanced steady state solution. Finally, we also run the same test cases with the classical WENO3 and WENO5 schemes.

Convergence curves for supercritical and subcritical flows are depicted in Figures 6 and 7, respectively. All curves, both for WENO3 and WENO5, show the correct third and fifth order accuracy. However, it should be noticed that the GF formulation allows a much better prediction of the solution characterized by a discretization error that is by far lower compared to the classical method. Introducing then the WB formulation allows even better convergence trends with slightly lower errors with the advantage of preserving also the lake-at-rest solution. In some cases, e.g. supercritical flow GF-WENO5 WB and GF-WENO3 non-WB, we observe a superconvergence of the methods, which might be caused by the extra constraints that the flux globalization and WB techniques impose. The behavior is still under investigation.

After the convergence analysis, we focus on a more qualitative analysis of the results computed with the WENO5 and GF-WENO5 methods. To do so we introduce a set of four representative variables that we are

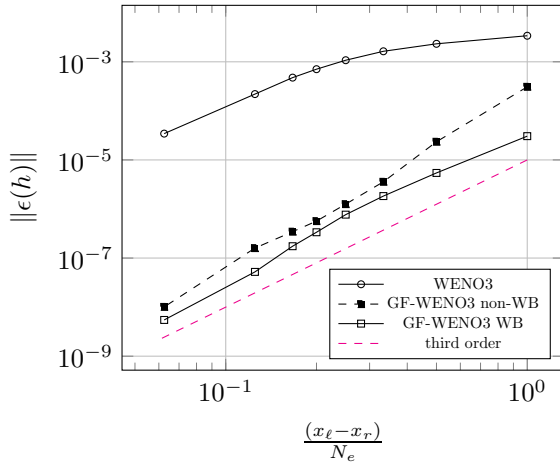


(a) WENO3

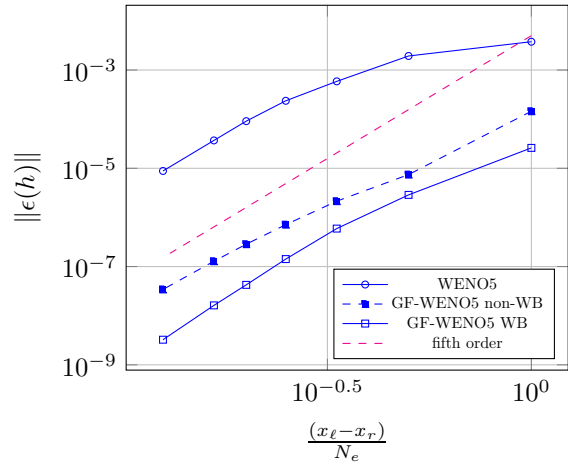


(b) WENO5

Figure 6: Supercritical flow: convergence tests with WENO3 and WENO5.



(a) WENO3



(b) WENO5

Figure 7: Subcritical flow: convergence tests with WENO3 and WENO5.



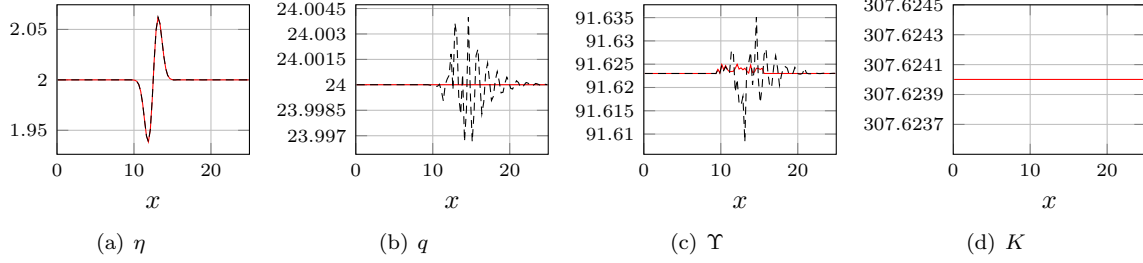


Figure 8: Supercritical flow: relevant variables computed with GF-WENO5 (red continuous line) and WENO5 (black dashed line) schemes.

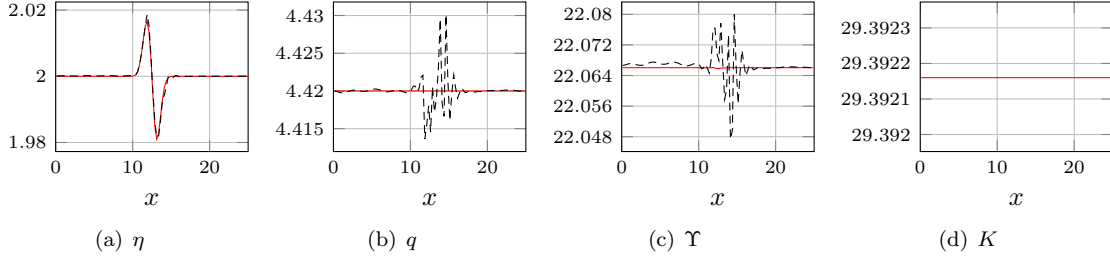


Figure 9: Subcritical flow: relevant variables computed with GF-WENO5 (red continuous line) and WENO5 (black dashed line) schemes.

going to use to compare the classical WENO5 with the new GF-WENO5 WB. The three main variables that we used to assess the new method are  $\eta$ ,  $q$  and  $K$  ( $K$  is only defined for GF formulation). In particular, it should be noticed that, by construction, the methods based on flux globalization preserve moving equilibria, i.e.,  $q_x \equiv 0$ ,  $K_x \equiv 0$ . This means that the GF-WENO5 will approximate these quantities up to the order of the residual of the time derivative at the end of the simulation. In our case, we are able to preserve the constant  $q$  and  $K$  up to  $\sim 10^{-9}$ . The last variable we decided to study is the aforementioned  $\Upsilon$ , which corresponds to the smooth formulation of the more general global flux introduced herein. Although our approach is developed to preserve other equilibria, this variable allows to get more insights about the capability of the new algorithm since, for smooth flows, the analytical  $\Upsilon$  should be constant at equilibrium. Solutions for supercritical and subcritical flows are shown in Figures 8 and 9. For both cases, it is clear that  $q$  and  $K$  are well-preserved, and  $\Upsilon$  is much better predicted with respect to the one computed through the classical WENO5 method. The test case that stands out more among the three situation considered here is the transcritical flow with shock in Figure 10. The WENO5 method introduces spurious oscillation where the shock occurs that are then propagated in the rest of the computational domain making the overall solution spoiled. By using the new GF-WENO5 approach, oscillations are not present and the correct solution is recovered before and after the shock. It can be noticed that, when discontinuous flows are of interest,  $\Upsilon$  is not globally constant but features a jump where the shock occurs, see Figure 10.

#### 5.4 Steady states with friction ( $n = 0.05$ )

In this section we focus on the supercritical and subcritical flows studied in Section 5.3 including the friction term in the source term. As for the previous cases, also when friction with constant Manning coefficient  $n$  is present, we can obtain moving equilibria. Again the quantity that are preserved at equilibrium are  $q$  and  $K$ . That is why it is interesting to perform simulations similar to the previous ones comparing standard methods with GF ones.

We consider the subcritical case defined in (70) and the supercritical case defined in (71) with the same

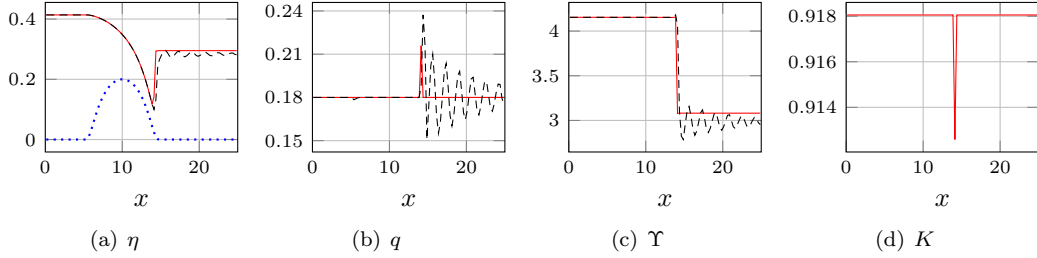


Figure 10: Transcritical flow: relevant variables computed with GF-WENO5 (red continuous line), WENO5 (black dashed line) schemes and  $b$  (blue dotted line).

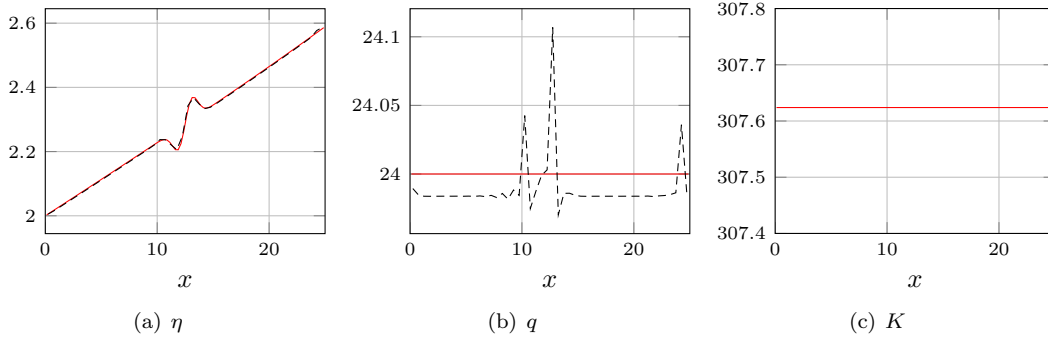


Figure 11: Supercritical flow with friction: relevant variables computed with GF-WENO5 (red continuous line) and WENO5 (black dashed line) schemes.

bathymetry, on which we add the friction term with Manning coefficient  $n = 0.05$ . In the supercritical case, the friction term implies a slow down of the physical speed from left to right and a consequent increasing of  $\eta$  from left to right. In the subcritical case, conversely, we expect  $h$  to decrease from left to right and the speed to increase. The variable  $\Upsilon$  is not conserved and, for these tests, there is not another constant variable that can be easily computed analytically, hence, we do not plot it.

We display in Figures 11 and 12 both the solutions computed with the new GF-WENO5 WB scheme and the classical WENO5. It should be noticed that both schemes obtain valid and consistent results with the expected solution. The difference between the schemes is remarkable and the global flux variables clearly highlights it. The WENO5 case, without the global flux, is characterized by strong spurious oscillations around the area where the effect of the bathymetry is stronger. On the other side, the GF-WENO5 results are very precise and are able to preserve the global flux variables up to  $\sim 10^{-9}$ .

## 6 Conclusion

In this paper, we presented a novel arbitrary high-order well-balanced finite-volume method based on flux globalization for the shallow water equations with source terms. The high order accuracy is obtained through a WENO reconstruction performed on the variables of interest, i.e. free surface level and global fluxes. The flux globalization allows to exactly preserve the constant fluxes in moving water equilibria. The new scheme has been also designed to preserve the “lake-at-rest” solution. This was possible by introducing a particular quadrature procedure for the source flux and considering a jump of the global fluxes at each interface. Several tests have been performed to assess the properties of the scheme. The preservation of the constant flux has been verified on academic moving water test cases (subcritical, transcritical and supercritical), while the well-balancedness with respect to the lake at rest equilibrium has been tested on the classical “lake-at-rest”

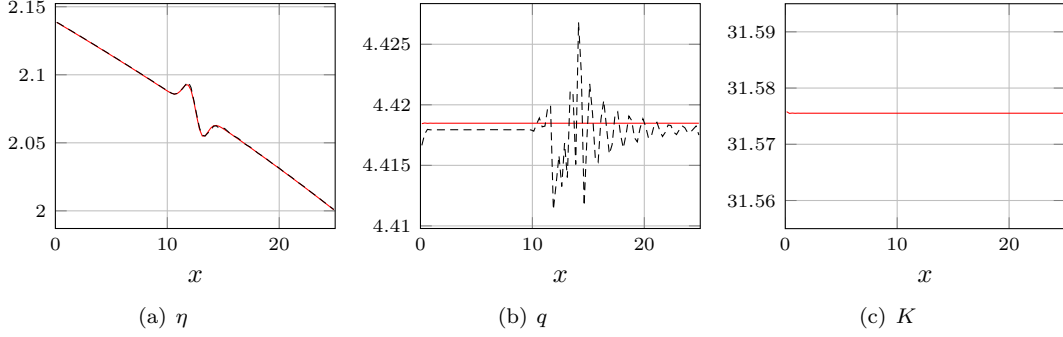


Figure 12: Subcritical flow with friction: relevant variables computed with GF-WENO5 (red continuous line) and WENO5 (black dashed line) schemes.

and “perturbed lake-at-rest” cases. Once the space discretization is well implemented, the introduction of additional source terms is straightforward, e.g. Manning friction, as demonstrated in the simulation section. With the presented scheme, we were able to outperform classical methods in many situations, obtaining much more accurate solutions and useful properties also at the discrete level. Moreover, the high order accuracy of scheme allows to obtain precise solutions also when the equilibria are not reached.

There are several extensions to this work that could be carried out. The authors are already studying a DGSEM-like formulation to simplify the global flux procedure, more complicated balance laws where other moving equilibria are object of interest, multi-dimensional problems on which the global flux must be carefully defined, and path-conservative strategies.

## Acknowledgements

D. T. has been funded by a postdoctoral fellowship in the CARDAMOM team in INRIA–Bordeaux Sud–Ouest and by a postdoctoral fellowship in SISSA. M. Ciallella is funded by an Inria PhD fellowship in the CARDAMOM team in INRIA–Bordeaux.

## A Positive reconstruction of water height at interfaces

From the cell average a high order WENO reconstruction is performed on the fluxes to have  $q_{i+1/2}^{L,R}$  and  $K_{i+1/2}^{L,R}$ . Equipped with  $q_{i+1/2}^{L,R}, K_{i+1/2}^{L,R}, \mathcal{R}_{i+1/2}^{L,R}$ , the point values  $h_{i+1/2}^{L,R}$  can be obtained by solving the nonlinear equation coming from the definition of the global variable  $K$  in (3):

$$K_{i+1/2}^L = \frac{(q_{i+1/2}^L)^2}{h_{i+1/2}^L} + \frac{g}{2} (h_{i+1/2}^L)^2 + \mathcal{R}_{i+1/2}^L, \quad K_{i+1/2}^R = \frac{(q_{i+1/2}^R)^2}{h_{i+1/2}^R} + \frac{g}{2} (h_{i+1/2}^R)^2 + \mathcal{R}_{i+1/2}^R \quad (73)$$

Let us solve the depressed cubic equation (73) for  $h_{i+1/2}^L$  (the solution for  $h_{i+1/2}^R$  is obtained with the same procedure). First of all, it can be noticed that (73) does not have any positive solution unless the determinant is greater than zero, meaning that

$$(q_{i+1/2}^L)^4 < \frac{8 (K_{i+1/2}^L - \mathcal{R}_{i+1/2}^L)^3}{27g}. \quad (74)$$

If (74) is not satisfied we reconstruct  $\eta_{i+1/2}^L$  and then compute  $h_{i+1/2}^L$  given that

$$h_{i+1/2}^L = \eta_{i+1/2}^L - b_{i+1/2}^L. \quad (75)$$

If (74) is satisfied, then we have to deal with two possibilities. First, if  $q_{i+1/2}^L = 0$ , we obtain the unique positive solution

$$h_{i+1/2}^L = \sqrt{\frac{2 \left( K_{i+1/2}^L - \mathcal{R}_{i+1/2}^L \right)}{g}},$$

while if  $q_{i+1/2}^L \neq 0$ , we solve Eq. (73) for  $h_{i+1/2}^L$  and obtain the following three solutions:

$$h_{i+1/2}^L = 2\sqrt{P} \cos \left( \frac{1}{3} [\Theta + 2\pi k] \right), \quad k = 0, 1, 2, \quad (76)$$

where

$$P := \frac{2 \left( K_{i+1/2}^L - R_{i+1/2}^L \right)}{3g} \quad \text{and} \quad \Theta := \arccos \left( -\frac{\left( q_{i+1/2}^L \right)^2}{g P^{3/2}} \right). \quad (77)$$

It can be shown that one of these roots is negative, whilst the other two roots, corresponding to the subcritical and supercritical cases, are positive. We choose the one closer to the corresponding value of  $h_{i+1/2}^L$  given in (75).

## References

- [1] R. Abgrall. High order schemes for hyperbolic problems using globally continuous approximation and avoiding mass matrices. *Journal of Scientific Computing*, 73(2-3):461–494, 2017.
- [2] R. Abgrall, E. L. Mélédo, P. Öffner, and D. Torlo. Relaxation deferred correction methods and their applications to residual distribution schemes. *arXiv preprint arXiv:2106.05005*, 2021.
- [3] R. Abgrall and D. Torlo. High order asymptotic preserving deferred correction implicit-explicit schemes for kinetic models. *SIAM Journal on Scientific Computing*, 42(3):B816–B845, 2020.
- [4] L. Arpaia and M. Ricchiuto. r- adaptation for shallow water flows: conservation, well balancedness, efficiency. *Computers & Fluids*, 160:175–203, 2018.
- [5] L. Arpaia, M. Ricchiuto, A. G. Filippini, and R. Pedreros. An efficient covariant frame for the spherical shallow water equations: Well balanced DG approximation and application to tsunami and storm surge. *Ocean Modelling*, 169:101915, 2022.
- [6] E. Audusse, F. Bouchut, M.-O. Bristeau, R. Klein, and B. t. Perthame. A fast and stable well-balanced scheme with hydrostatic reconstruction for shallow water flows. *SIAM Journal on Scientific Computing*, 25(6):2050–2065, 2004.
- [7] D. S. Balsara and C.-W. Shu. Monotonicity preserving weighted essentially non-oscillatory schemes with increasingly high order of accuracy. *Journal of Computational Physics*, 160(2):405–452, 2000.
- [8] C. Berthon and C. Chalons. A fully well-balanced, positive and entropy-satisfying Godunov-type method for the shallow-water equations. *Mathematics of Computation*, 85(299):1281–1307, 2016.
- [9] A. Bollermann, G. Chen, A. Kurganov, and S. Noelle. A well-balanced reconstruction of wet/dry fronts for the shallow water equations. *Journal of Scientific Computing*, 56(2):267–290, 2013.
- [10] Y. Cheng, A. Chertock, M. Herty, A. Kurganov, and T. Wu. A new approach for designing moving-water equilibria preserving schemes for the shallow water equations. *Journal of Scientific Computing*, 80(1):538–554, 2019.

- [11] A. Chertock, S. Cui, A. Kurganov, Ş. N. Özcan, and E. Tadmor. Well-balanced schemes for the euler equations with gravitation: Conservative formulation using global fluxes. *Journal of Computational Physics*, 358:36–52, 2018.
- [12] A. Chertock, A. Kurganov, X. Liu, Y. Liu, and T. Wu. Well-balancing via flux globalization: Applications to shallow water equations with wet/dry fronts. *Journal of Scientific Computing*, 90(1):1–21, 2022.
- [13] A. Christlieb, B. Ong, and J.-M. Qiu. Integral deferred correction methods constructed with high order Runge-Kutta integrators. *Mathematics of Computation*, 79(270):761–783, 2010.
- [14] M. Ciallella, L. Micalizzi, P. Öffner, and D. Torlo. An arbitrary high order and positivity preserving method for the shallow water equations. *arXiv preprint arXiv:2110.13509*, 2021.
- [15] J. W. Daniel, V. Pereyra, and L. L. Schumaker. Iterated deferred corrections for initial value problems. *Acta Cient. Venezolana*, 19:128–135, 1968.
- [16] B. De Saint Venant. Theorie du mouvement non-permanent des eaux avec application aux crues des rivières et à l'introduction des marées dans leur lit. *Academic de Sci. Comptes Rendus*, 73(99):148–154, 1871.
- [17] O. Delestre, C. Lucas, P.-A. Ksinant, F. Darboux, C. Laguerre, T.-N.-T. Vo, F. James, and S. Cordier. Swashes: a compilation of shallow water analytic solutions for hydraulic and environmental studies. *International Journal for Numerical Methods in Fluids*, 72(3):269–300, 2013.
- [18] M. C. Díaz, J. A. López-García, and C. Parés. High order exactly well-balanced numerical methods for shallow water systems. *Journal of Computational Physics*, 246:242–264, 2013.
- [19] A. Dutt, L. Greengard, and V. Rokhlin. Spectral Deferred Correction Methods for Ordinary Differential Equations. *BIT Numerical Mathematics*, 40(2):241–266, 2000.
- [20] J. M. Gallardo, C. Parés, and M. Castro. On a well-balanced high-order finite volume scheme for shallow water equations with topography and dry areas. *Journal of Computational Physics*, 227(1):574–601, 2007.
- [21] S. K. Godunov. A difference scheme for numerical solution of discontinuous solution of hydrodynamic equations. *Math. Sbornik*, 47:271–306, 1959.
- [22] E. Hairer and G. Wanner. Solving ordinary differential equations. II, Vol. 14 of. *Springer Series in Computational Mathematics (Springer Berlin Heidelberg, Berlin, Heidelberg, 1996)*, 10:978–3, 1996.
- [23] M. Han Veiga, P. Öffner, and D. Torlo. DeC and ADER: Similarities, Differences and a Unified Framework. *Journal of Scientific Computing*, 87(1):1–35, 2021.
- [24] G.-S. Jiang and C.-W. Shu. Efficient implementation of weighted ENO schemes. *Journal of Computational Physics*, 126(1):202–228, 1996.
- [25] A. Kurganov. Finite-volume schemes for shallow-water equations. *Acta Numerica*, 27:289–351, 2018.
- [26] A. Kurganov and G. Petrova. A second-order well-balanced positivity preserving central-upwind scheme for the saint-venant system. *Communications in Mathematical Sciences*, 5(1):133–160, 2007.
- [27] Y. Liu, C.-W. Shu, and M. Zhang. Strong stability preserving property of the deferred correction time discretization. *Journal of Computational Mathematics*, pages 633–656, 2008.
- [28] M. Lukáčová-Medvid'ová, S. Noelle, and M. Kraft. Well-balanced finite volume evolution Galerkin methods for the shallow water equations. *Journal of Computational Physics*, 221(1):122–147, 2007.

- [29] Y. Mantri and S. Noelle. Well-balanced discontinuous Galerkin scheme for  $2 \times 2$  hyperbolic balance law. *Journal of Computational Physics*, 429:110011, 2021.
- [30] A. Meister and S. Ortleb. On unconditionally positive implicit time integration for the DG scheme applied to shallow water flows. *International Journal for Numerical Methods in Fluids*, 76(2):69–94, 2014.
- [31] V. Michel-Dansac, C. Berthon, S. Clain, and F. Foucher. A well-balanced scheme for the shallow-water equations with topography. *Computers & Mathematics with Applications*, 72(3):568–593, 2016.
- [32] V. Michel-Dansac, C. Berthon, S. Clain, and F. Foucher. A well-balanced scheme for the shallow-water equations with topography or manning friction. *Journal of Computational Physics*, 335:115–154, 2017.
- [33] V. Michel-Dansac, C. Berthon, S. Clain, and F. Foucher. A two-dimensional high-order well-balanced scheme for the shallow water equations with topography and manning friction. *Computers & Fluids*, 230:105152, 2021.
- [34] M. L. Minion. Semi-implicit spectral deferred correction methods for ordinary differential equations. *Commun. Math. Sci.*, 1(3):471–500, 09 2003.
- [35] S. Noelle, Y. Xing, and C.-W. Shu. High-order well-balanced finite volume WENO schemes for shallow water equation with moving water. *Journal of Computational Physics*, 226(1):29–58, 2007.
- [36] M. Ricchiuto. On the C-property and generalized C-property of residual distribution for the shallow water equations. *Journal of Scientific Computing*, 48(1):304–318, 2011.
- [37] M. Ricchiuto. An explicit residual based approach for shallow water flows. *Journal of Computational Physics*, 280:306–344, 2015.
- [38] M. Ricchiuto, R. Abgrall, and H. Deconinck. Application of conservative residual distribution schemes to the solution of the shallow water equations on unstructured meshes. *Journal of Computational Physics*, 222(1):287–331, 2007.
- [39] M. Ricchiuto and A. Bollermann. Stabilized residual distribution for shallow water simulations. *Journal of Computational Physics*, 228(4):1071–1115, 2009.
- [40] C.-W. Shu. Essentially non-oscillatory and weighted essentially non-oscillatory schemes for hyperbolic conservation laws. In *Advanced numerical approximation of nonlinear hyperbolic equations*, pages 325–432. Springer, 1998.
- [41] C.-W. Shu and S. Osher. Efficient implementation of essentially non-oscillatory shock-capturing schemes. *Journal of Computational Physics*, 77(2):439–471, 1988.
- [42] D. Torlo. *Hyperbolic problems: high order methods and model order reduction*. PhD thesis, PhD thesis, University Zurich, 2020.
- [43] Y. Xing and C.-W. Shu. A survey of high order schemes for the shallow water equations. *J. Math. Study*, 47(3):221–249, 2014.